DYNAMICS IN LARGE MOLECULES, CLUSTERS, CONDENSED PHASE AND BIOMOLECULES

JOSHUA JORTNER
School of Chemistry, Tel-Aviv University
Ramat Aviv, 69978 Tel Aviv, Israel

ABSTRACT

This paper reviews the conceptual framework of femtosecond chemistry which rests on the theory and simulation of intramolecular, cluster, condensed phase and biophysical dynamics.

1. Prologue

We shall be concerned with femtosecond dynamics in large isolated molecules, clusters, condensed phase and biosystems, which pertains to the elucidation of the phenomena of energy acquisition, storage and disposal as explored from the microscopic point of view.

The advent of femtosecond dynamics[1,2] opened up new horizons in the exploration of ultrafast nonradiative processes. In this context we should inquire: How fast is ultrafast? This question attracts different answers in different areas of science (Fig. 1). In the realm of molecular and condensed phase dynamics, ultrafast relaxation prevails on the time scale of nuclear motion. This is the case for isolated molecules where ultrafast 'nonreactive' intramolecular internal conversion can occur on the time scale of vibrational motion, while 'reactive' dissociation[3,4] and Coulomb explosion[5,6] manifest the sliding down on the repulsive nuclear surface. In some cluster and condensed phase systems ultrafast energy dissipation processes, manifesting collective large nuclear configurational changes, bear analogy to molecular 'reactive' dynamics, but can concurrently maintain vibrational phase coherence induced by nuclear impact. For ultrafast dynamics in clusters, in the condensed phase and in the protein medium, separation of time scales for nuclear dynamics may prevail.[5] Interstate and energy relaxation are understood, while the interplay between relaxation and dephasing is of considerable interest The ubiquity of vibrational and electronic coherence effects, ranging from small to huge systems,[2,7-9] raises the conceptual question of the distinction between the experimental conditions of the preparation and interrogation, and the intrinsic aspects of relaxation and dephasing dynamics. These are some of the central aspects of the novel and fascinating area of femtochemistry, whose conceptual framework rests on the theory and simulation of intramolecular, cluster, condensed phase and biophysical dynamics.

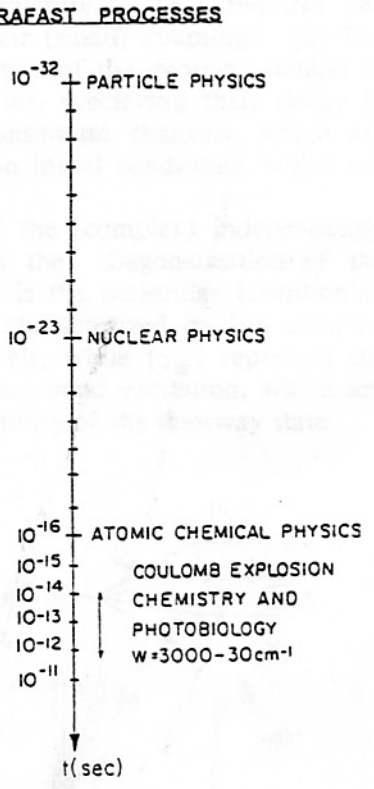

2. Intramolecular Dynamics

We start from the genesis of modern intramolecular dynamics. In 1965 the research area of intramolecular dynamics in large isolated molecules originated from the seminal experiments of Kistiakowski and Parmenter, which demonstrated the occurrence of intersystem crossing in the 'isolated' collision-free benzene molecule.[10] The iconoclastic implications of the occurrence of irreversible relaxation in a bound level structure were fully realized by Kistiakowski and Parmenter, who stated that their results may be incompatible with the laws of quantum mechanics.[10] The intramolecular nature of radiationless transitions in a bound level structure was established by the Bixon-Jortner model,[11-16] which rests on near-resonance coupling, on the dynamics of wavepackets of mixed bound states, on finite time evolution, and on the practical irreversibility in a dense bound level structure of a vibrational quasicontinuum. This general conceptual framework[11-20] is applicable both for interstate coupling, which involves two electronic configurations coupled by nuclear momenta (i.e., the breakdown of Born-Oppenheimer separability) or/and spin-orbit interaction, as well as for intrastate coupling, which involves a single electronic configuration with vibrational-rotational states coupled by anharmonic or coriolis interactions.

The central ingredients of the theory of intramolecular dynamics in a bound level structure are: (1) The characterization of the level structure. This requires the characterization of the appropriate zero-order states and their (small) couplings. (2) The accessibility of the zero-order states, leading to the specification of the doorway state(s) of the system. (3) The decay channels of the zero-order states, specifying their decay to genuine (radiative decay, predissociation, autoionization) continuum channels, which are characterized by appropriate decay widths. (4) The excitation initial conditions, which are governed by the (optical) excitation modes.

Ingredients (1) and (3) allow for the construction of the (complex) independently decaying molecular levels $\{|m\rangle\}$, which are obtained from the diagonalization of the effective Hamiltonian[15-18,20] $\underset{\approx}{H}_{eff} = \underset{\approx}{H}_M - (i/2)\underset{\approx}{\Gamma}$, where $\underset{\approx}{H}_M$ is the molecular Hamiltonian and $\underset{\approx}{\Gamma}$ is the decay matrix (Fig. 2). The $\{|m\rangle\}$ states are characterized by the complex energies $\underset{\approx}{\epsilon}_m = E_m - (i/2)\gamma_m$, where $\{E_m\}$ are the energy levels, while $\{\gamma_m\}$ represent the decay widths. Relevant time-resolved observables for a broad-band excitation, which are based on ingredients (1) and (2), involve the population probability of the doorway state

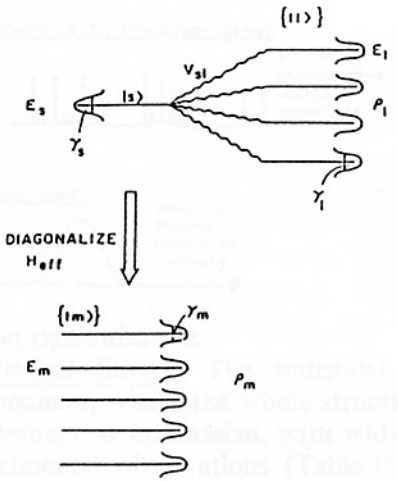

Fig. 2 The application of the effective Hamiltonian formalism for interstate and intrastate intramolecular coupling and dynamics. The zero-order states $|s\rangle$ and $\{|\ell\rangle\}$ are characterized by the energies E_s and $\{E_\ell\}$, respectively, and by the decay widths γ_s and $\{\gamma_\ell\}$. $V_{s\ell}$ represents the intramolecular (interstate or intrastate) coupling between the doorway state $|s\rangle$ and the $\{|\ell\rangle\}$ manifold, which is characterized by the density of states ρ_ℓ. Diagonalization of the effective Hamiltonian results in a set of independently decaying levels $\{|m\rangle\}$, i.e., generalized molecular eigenstates, characterized by energies $\{E_m\}$, decay widths $\{\gamma_m\}$, and density of states ρ_m.

$$P^{(D)}(t) = |\sum_m |A_m|^2 \exp\left(\frac{-iE_m t}{\hbar} - \frac{\gamma_m t}{2\hbar}\right)|^2 \quad , \tag{1}$$

where $A_m = \langle g|\hat{\mu}|m\rangle$ are the excitation amplitudes of the $\{|m\rangle\}$ manifold, and the energy-resolved (radiative) decay probability to a vibrational level $|gv\rangle$ of the ground electronic state

$$P^{(v)}(t) = |\sum_m A_m B^v_m \exp\left(\frac{-iE_m t}{\hbar} - \frac{\gamma_m t}{\hbar}\right)|^2 \quad , \tag{2}$$

where $B^v_m = \langle m|\hat{\mu}|gv\rangle$ are the transition amplitudes. These probabilities constitute Fourier sums damped by real decay exponents, Eq. (1), and may involve either a superposition of exponentials (for a sparse or intermediate level structure) or an exponential decay of a giant resonance (in the statistical limit), while Eq. (2) may also result in quantum beats (in the intermediate level structure). The character and dynamical manifestations of the sparse, intermediate and statistical level structures (Fig. 2) can be inferred in a transparent way from the lineshapes $L(E) = -\mathrm{Im}G(E)$, where the Green's function is $G(E) = (E-H_{eff})^{-1}$. The classification of the level structures (Fig. 1) is specified by the coarse grained (interstate or intrastate) coupling V, by the density of states of the proper symmetry ρ, and by the decay widths γ. The limit of isolated states (case 1), with $V\rho < 1$, constitutes the spectroscopist's paradise, when distinct 'pure' rotational-vibrational levels can be observed. For the strongly coupled situation, with $V\rho > 1$, the sparse ($\gamma\rho < 1$), the intermediate ($\gamma\rho \sim 1$) and the statistical ($\gamma\rho >> 1$) level structures, (Fig. 3), can be realized.

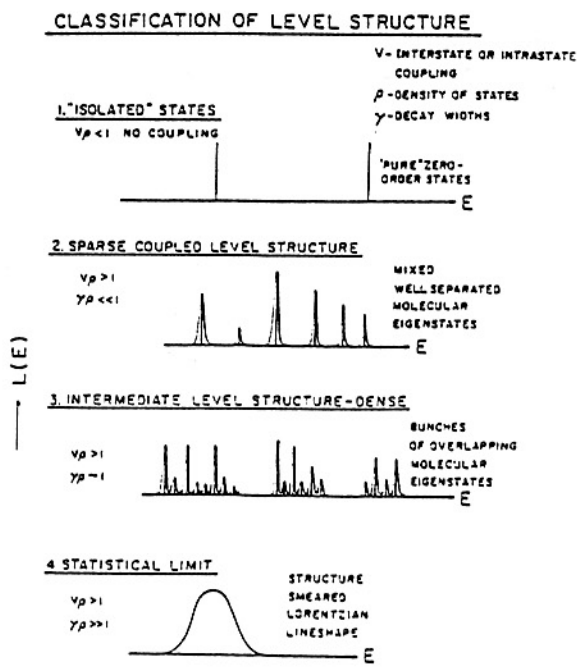

Fig. 3. Classification of the intramolecular level structure. The relevant energetic and dynamic parameters are: the (interstate or intrastate) coupling V, the density of the independently decaying levels ρ and their decay widths γ. The spectra exhibit the energy dependent linewidth L(E) vs E.

Some aspects of the theory relevant to femtosecond dynamics are:

(1) Ultrafast intramolecular relaxation in the statistical limit. The statistical limit corresponds to the extreme situation of overlapping resonances, where the whole structure in the spectrum is washed out (Fig. 3). The absorption lineshape is Lorentzian, with width $\Gamma = 2\pi\Sigma_\ell |V_{s\ell}|^2 \delta(E_s - E_\ell)$ and lifetime $\tau = \hbar/\Gamma$. The experimental observations (Table I) of a Lorentzian absorption lineshape of the electronic origins (which preclude IVR) of

intravalence and Rydberg excitations of large isolated jet-cooled molecules (explored at Tel Aviv), constitutes the victory of dynamics over spectroscopy for a highly congested bound level structure. This spectroscopic information on ultrafast intramolecular dynamics ($\tau \simeq$ 3000-20 fsec) has to be supplemented by time-resolved information.

Table I. Electronic Relaxation Lifetimes in Isolated Jet-Cooled Molecules

Molecules	Channels	τ(fs)
Azulene	$S_1 \rightarrow S_0$	800 ± 200
S_1	$\Delta E = 14400\ cm^{-1}$	
Phenantrene	$S_2 \rightarrow S_1$	500 ± 100
S_2	$\Delta E = 4684\ cm^{-1}$	
Free-Base	$S_2 \rightarrow S_1$	450 ± 50
Porphin S_2(Qy)	$\Delta E = 3540\ cm^{-1}$	
Zn-tetraphenyl	$S_2 \rightarrow S_1$	3200 ± 300
Porphyrin	$\Delta E = 9050\ cm^{-1}$	
Benzene (H_6) n=3	$3nRy \rightarrow \{S_n\} \rightarrow S_0$	160
Rydberg Benzene (D_6)		190
Benzene	S_3 + Dissociative channels	(20)

(2) Mode selectivity. The characteristics of interstate coupling and intramolecular relaxation can be more complex and interesting due to resonance effects.[21] Mediated intersystem crossing from a S_1 vibronic state to the dense lowest triplet $\{T_1\}$ manifold can be induced by the sequential coupling via a sparse manifold $\{T_x\}$ of vibronic states corresponding to a higher triplet state. The theory of mediated coupling and relaxation predicts the occurrence of resonances originating from $\{T_x\}$-$\{T_1\}$ vibronic coupling, which mediate the decay of the S_1 doorway state. When the level structure of the $\{T_x\}$-$\{T_1\}$ resonances is sparse, the decay rate is very sensitive to the energy gaps between the S_1 and the T_x states. Accordingly, climbing up the vibrational levels in the S_1 manifold above its electronic origin will result in a wide variation of their radiationless decay rates, exhibiting a marked mode selectivity of mediated intersystem crossing. Such dramatic vibrational mode-selective effects are revealed in the absolute fluorescence quantum yields from photoselected vibronic levels in the S_1 manifold of 9,10 dibromoanthracene,[21] (Fig. 4), where the irregular variance of the nonradiative lifetimes spans about three orders of magnitude. These resonance effects for the decay of the S_1 state span the excess vibrational energy range E_{vib} = 0-800 cm^{-1} above the electronic origin of the S_1 electronic manifold, while at higher E_{vib} mode selectivity is eroded due to intramolecular vibrational energy redistribution.

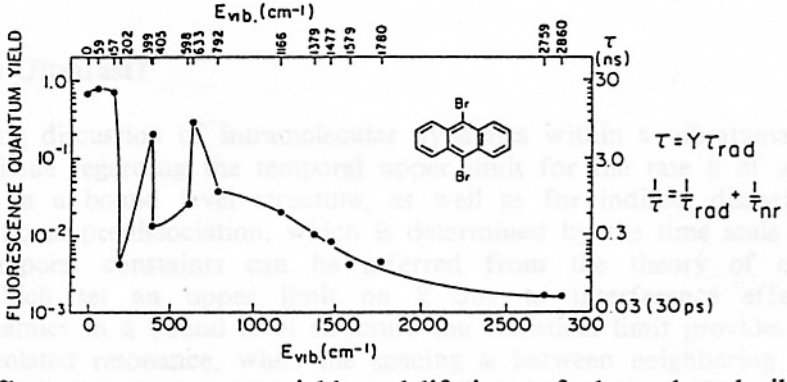

Fig. 4. Absolute fluorescence quantum yields and lifetimes of photoselected vibronic level of jet-cooled 9,10 dibromoanthracene,[21] which exhibit a marked mode selectivity in the vibrational energy range $0 \leq E_{vib} \leq 800\ cm^{-1}$ above the electronic origin.

(3) Towards chemistry. Long-range electron transfer (ET) in isolated supermolecules. ET reactions in chemistry, physics and biology have been almost exclusively explored in donor (D) - acceptor (A) systems embedded in a medium, e.g., solvent, glass or protein. Nonradiative ET can be realized as an intramolecular radiationless transition. We have challenged the conventional wisdom regarding the dominating role of medium coupling in ET, proposed that long-range ET occurs in isolated solvent-free supermolecules and analysed the structural constraints for the occurrence of this radiationless transition.[22-24] ET rates were given in the statistical limit in the form $k_j = (2\pi/\hbar)\Sigma_f |\langle j|H|f\rangle|^2 \delta(E_j - E_f)$ in terms of products of electronic coupling and nuclear Franck-Condon overlap. The theory allows for the quantification of the ladder diagram. Isolated molecule ET rates exhibit the energy gap (ΔE) dependence, (Fig. 5), with typical ET rates in the range $k_j = 10^{11}$-5×10^{12} sec^{-1} for charge separation from the electronically excited state. This analysis builds a bridge between ET and intramolecular radiationless transitions, reflecting on the universal unifying features of intramolecular and medium induced relaxation.

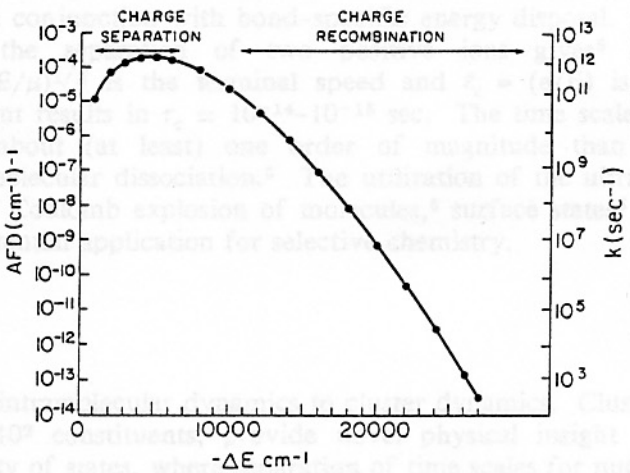

Fig. 5. ET dynamics in isolated supermolecules. The energy gap ($-\Delta E$) dependence of the averaged Franck-Condon density AFD and the rate $k = (2\pi/\hbar)V^2(AFD)$ ($V = 100\ cm^{-1}$) for the electronic origin. Calculations for a $n = 4$ intramolecular vibrational level system $(\omega/cm^{-1}) = (200, 500, 1200, 1500)$ with couplings $S = (6, 3, 1, 1)$. Note the exponential energy gap at large $-\Delta E$.

(4) The electronic quasicontinuum. Very high n (= 50-250) molecular Rydberg states are characterized by a high density ($\rho \propto n^3/Ry$) of electronic states and unique $n\ell$-$n'\ell'$ multipole core-electron interactions. A generalization of the theory of intramolecular coupling and dynamics was provided for an electronic quasicontinuum.[25]

3. How Fast Is Ultrafast?

The preceding discussion of intramolecular dynamics within a vibrational manifold raises the central issue regarding the temporal upper limit for the rate k of an ultrafast relaxation process in a bound level structure, as well as for indirect dissociation, i.e., electronic or vibrational predissociation, which is determined by the time scale of nuclear motion. The temporal constaints can be inferred from the theory of overlapping resonances,[26,27] which set an upper limit on k due to interference effects. For intramolecular dynamics in a bound level structure the statistical limit provides the decay rate $\Gamma/\hbar$ for an isolated resonance, when the spacing ω between neighboring resonances exceeds Γ. Provided that the coupling to the quasicontinuum is sufficiently 'smooth' (determined by correlation between individual coupling terms) interference effects will set in when $\Gamma \sim \omega$. The intramolecular relaxation rate is[26,27] $k \simeq (\Gamma/\hbar)[1+(\pi\Gamma/\omega)]^{-1}$, whereupon $k = \Gamma/\hbar$ for $\Gamma << \omega$ and $k = \omega/\hbar$ for $\Gamma >> \omega$. The overlapping resonance domain provides an

upper limit for the rate, which is determined by the level spacing ω, i.e., the vibrational frequency. The transition from $k = \Gamma/\hbar$ for isolated resonances to $k = \omega/\hbar$ for overlapping resonances is expected to prevail also for indirect dissociation, i.e., electronic and vibrational predissociation.

For direct dissociation in 'small' molecular systems the dynamics involves the sliding on a repulsive potential surface.[3,4] The characteristic time for dissociation is described in terms of a classical mechanical model of Zewail and his colleagues[3,4]

$$\tau_c = \int_{R_0}^{R} \frac{dR'}{v(R')} \quad , \tag{3}$$

where $v(R')$ is the velocity at R'. The time scale for direct dissociation is $\tau_c \simeq 10^{-13}$ sec.

An ultrafast excitation leading to the localization of energy in polyatomic molecules or clusters can be achieved by a Coulomb explosion.[5,6] This ultrafast process is characterized by site selective energy acquisition in conjunction with bond-specific energy disposal. The mechanical model, Eq. (3), for the separation of two positive ions gives[5] $\tau_c \simeq (\ell_c/2\nu_c)\ell n(4<R>/\ell_c)$, where $\nu_c = (2E/\mu)^{1/2}$ is the terminal speed and $\ell_c = (e/E)$ is the terminal length. This simple argument results in $\tau_c \simeq 10^{-14}$–10^{-15} sec. The time scale for Coulomb explosion is shorter by about (at least) one order of magnitude than the corresponding time scale for direct molecular dissociation.[5] The utilization of the ultrafast (10^{-14}–10^{-15} sec) "chemical clock" of Coulomb explosion of molecules,[5] surface states[5] and clusters[6] precludes IVR and shows potential application for selective chemistry.

4. Large Finite Systems

We proceed from the world of intramolecular dynamics to cluster dynamics. Clusters, i.e., finite aggregates containing 2–10^9 constituents, provide novel physical insight into dynamics in systems with finite density of states, where separation of time scales for nuclear motion can be realized.[5,28] A key concept for the quantification of the unique characteristics of clusters pertains to size effects.[28] These involve the evolution of structural, thermodynamic, electronic, energetic, electrodynamic and dynamic features of finite systems with increasing the cluster size. Regarding dynamic cluster size effects, of considerable interest are:

(1) The 'transition' from molecular type dissociative dynamics in small clusters to condensed matter type nonreactive vibrational relaxation in large clusters, manifesting the bridging between molecular and condensed phase nuclear dynamics.[28]

(2) Collective vibrational modes. Interior, collective, compression nuclear modes of molecular clusters (He_n, Ar_n) can be treated in terms of the excitation of a liquid drop[29] and were experimentally documented.[30] Complementary to the energetics of these collective modes, their dynamics is interesting. The damping of the collective motion via the coupling of a 'giant resonance' to non-coherent vibrational modes, constitutes a theoretical and experimental challenge.

(3) Ultrafast energy acquisition via high-energy cluster-wall collisions. High-energy impact of atomic or molecular cluster ions (of sizes of 10–1000 constituents, with velocities up to ~ 20 km s^{-1} and kinetic energies up to ~ 100 eV per particle) on insulator, semiconductor or metal surfaces, produces a new medium of extremely high density (up to ~ 4 times the standard density), high temperature (up to ~ 10^5 K) and high energy density (up to 10^2 eV per particle), which is temporarily generated during the propagtion of a microshock wave within the cluster on the 10^2–10^3 femtosecond time scale.[31] Chemical applications, e.g.,

cluster impact dissociation of a probe diatomic molecule, were attempted.[31] The dissociation process is limited by the vibrational period of the molecule. Cluster impact dynamics opens up a new research area of thermal femtosecond chemistry.

These are some novel features of ultrafast cluster nuclear dynamics. Of considerable interest is the dynamics of large local configurational charge induced by an extravalence excitation of a probe atom (e.g., $^1S_0 \rightarrow {}^3P_1$ excitation of Xe) or molecule (e.g., Rydberg excitation of NO) in a rare-gas cluster. Molecular dynamics simulations of the dynamics of configurational nuclear relaxation around the $^3P_1$ excitation of Xe located in the central site in $XeAr_n$ clusters (Fig. 6) reveals the following features:[32] (1) Large configurational dilation, i.e., "bubble" formation on the time scale of $t_B \sim 300$-500 fsec. (2) t_B marks the time scale for ultrafast energy transfer. (3) Multimodal time evolution, with slower time scales of 3-5 psec. (4) Marked impact vibrational coherence effects. This vibrational coherence (Fig. 6) characterizes the collective vibrations around the excited probe atom with a long time scale for dephasing of > 5 psec. Thus vibrational coherence in the n = 146 cluster survives on a time scale considerably exceeding the initial configurational relaxation time.

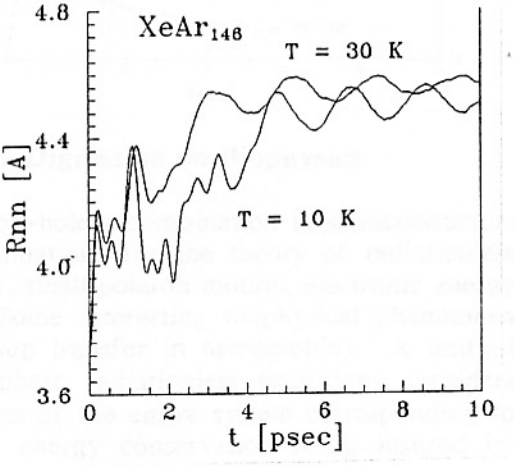

Fig. 6. The time evolution of the average Xe-Ar distance R_{nn} of $Xe(^3P_1)$ at the central site in $XeAr_{146}$.[32] T = 10K, 30K mark the equilibrium cluster temperature prior to excitation. Configurational dilation is manifested by the increase of R_{nn} on the time scale of ~ 300 fsec. Note the impact vibrational coherence manifested by oscillations in R_{nn}.

5. Dynamics of Electron Bubbles

The local configurational changes in clusters (and in the condensed phase) can be greatly spatially amplified for excess electron localization in liquid helium.[33] The energetic instability (due to strong e-He repulsion) of the conduction band quasifree excess electron state leads to the formation of the electron bubble, with the electron being confined to a cavity with a radius of $R_b = 17$Å (at P = 0) in the liquid.[33] Since its experimental discovery in 1959, a wealth of information was assembled on the structure, large compressibility, transport, energetics and spectroscopy of this electron bubble. Of considerable interest is the dynamics of the electron bubble formation in liquid He. We considered[34] the adiabatic process where the strongly repulsive electron-helium interaction drives out a large number of atoms towards regions where the excess electron density is low, while the electron is localized within the fluid dilation where the helium density is negligible. The adiabatic electron bubble dynamics was described by a hydrodynamic model.[34] The cavity expansion time from the initial cavity radius R_0 to the radius R is $\tau(R) = \int_{R_0}^{R} dR'/V(R')$, where V(R') is the velocity of the cavity boundary, which is determined by the total change of the (electronic, surface, volume) free energy and by the fluid density. The expression for $\tau(R)$ is analogous to Eq. (3) for molecular dissociation and Coulomb explosion. For liquid ^{4}He the expansion time for the attainment of the equilibrium bubble radius is $R_b = 3.9$ ps (at P = 0). Predictions for the experimental observations of this new class of these dynamic processes emerged from the time evolution of $1s \rightarrow 1p$ and $1s \rightarrow 2p$ absorption spectra (Fig. 7). The adiabatic electron bubble expansion corresponds to a dynamic solvation

process of an excess electron in liquid He. In contrast to the solvation dynamics of an excess electron or of a giant dipole in polar solvents, which is dominated by short-range short-time angular relaxation of the solvent molecules driven by inertial motion, the electron bubble formation in liquid He involves a short-time radial expansion process.[34] This model provides the condensed phase analogy to the ultrafast dissociative molecular dynamics for sliding on a repulsive potential surface (section 3).

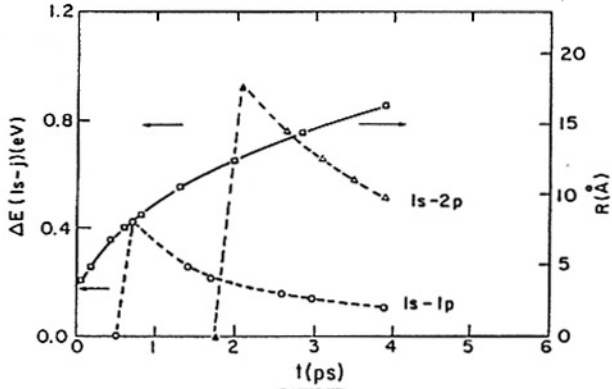

Fig. 7. The time evolution of the vertical transition energies ΔE (dashed curves) for the bound-bound $1s \rightarrow 1p$ and $1s \rightarrow 2p$ transitions of the electron bubble in liquid He. The time dependence of the bubble radius R (solid curve) is also shown.[34]

6. Multiphonon Nonadiabatic Processes and a Digression on Biophysics

The pioneering studies by Kubo[35] on electron-hole recombination in semiconductors and by Marcus on ET in solution[36] laid the foundations for the theory of radiationless electronic processes in the condensed phase (i.e., ET, small polaron motion, electronic energy transfer, high spin - low spin interconversion). Some interesting biophysical phenomena also fall in this category (ET in proteins and group transfer in hemoglobin). A unified conceptual framework for all these condensed phase radiationless transitions considers population relaxation between two potential surfaces of the entire system corresponding to distinct zero-order electronic configurations with energy conservation being insured by absorption and emission of phonons.[20] W_I for a nonradiative process from a reactant vibronic state $|I\rangle$ to the vibronic manifold$\{|J\rangle\}$ of product states quasidegenerate with it, is given by the golden rule expression $W_I = (2\pi/\hbar)|Ve|^2\Sigma_J|\langle I|J\rangle|^2\delta(E_I - E_J)$, where Ve is the appropriate electronic coupling. A basic assumption underlying the microscopic description of multiphonon nonadiabatic processes is the insensitivity of microscopic rates to the medium dynamics, which can be realized under one of the following conditions: (i) The common situation of fast medium vibrational dynamics, which allows the separation of time scales, with the microscopic ET rate constants constituting the rate determining step. Under these circumstances the rate W is expressed in terms of a thermal average $W = \Sigma_I P_I W_I$, where P_I is the thermal population of level $|I\rangle$. (ii) The microscopic rates depend weakly on the initial vibronic manifold. Under these circumstances $W \simeq W_I$. The dynamics is then analogous to the intramolecular statistical limit. Such a state of affairs prevails for activationless ET, where the potential surfaces cross in the vicinity of the minimum of the initial state, which pertains to the optimization of the ET rate.

The experimental exploration of ultrafast nonradiative processes in the condensed phase started 20 years ago for ET in a membrane protein.[37] These first studies of the primary ET processes in photosynthesis[37] determined the time scales for the oxidation of the special pair P ($\tau < 10$ psec) and for the reduction of the quionone ($\tau \simeq 200$ ps). The seminal determination of the structure of the bacterial photosynthetic reaction center (RC) in 1985 (ref. 38) led to a metamorphosis in the study of photosynthesis. Nevertheless, the basic issues which pertain to the dynamics of the primary charge separation, are not yet elucidated. The major limitations in the understanding of this central energy conversion

process in photobiology is that it requires information on the energetics, electronic interactions, and (intermolecular and intramolecular) nuclear dynamics, which cannot be inferred from the structural data in the ground electronic state. The outstanding problems in the understanding of the primary charge separation from $^1P^*$ to the bacteriopheophytin (H) are:

(A) Mechanisms. All mechanisms proposed attribute a special role to the accessory bacteriochlorophyl B, which may involve a one-step superexchange mechanism,[39] a two-step sequential mechanism via the P^+B^-H intermediate,[40] or the parallel sequential-superexchange mechanism (PSSM).[41,42] The PSSM has been successful in accounting for the kinetics of the primary charge separation in a series of mutants (which modify the energetics of $^1P^*$) and of chemically engineered RCs (Fig. 8). We inferred[41,42] that both ET routes prevail. The biological function of the native RC of photosynthetic bacteria at room temperature is dominated by the sequential mechanism. The superexchange route enables the prevalence of ET in mutants and chemically engineered RCs with extreme values of the energy gap. The PSSM implies a necessary kinetic redundancy, acting as a safety valve for energy changes and insuring the stability of the primary photosynthetic process for different native and mutagenetically modified RCs.

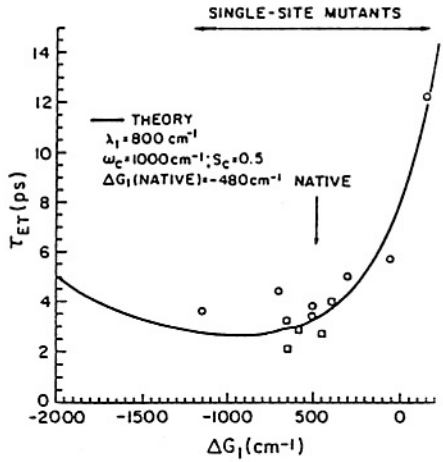

Fig. 8. Theoretical curve fitting the free energy relationship for the rate (T = 295 K) of the decay of $^1P^*$ in the native RC and some of its single site mutants (which modify ΔG_1 for the $^1P^*/P^+$ energetics). The theoretical curve presents the nonadiabatic multiphonon theory for sequential ET, which involves protein and intramolecular nuclear modes.[41]

(B) Symmetry breaking. The remarkable unidirectionality of the primary charge separation across a single (A) branch of the RC [39] is attributed to the cumulative contributions of the electronic coupling and of the nuclear Franck-Condon factors (originating from the $^1P^*$-P^+B^-H energetics) with both classes of effects reinforcing the branching ratio for ET across the A branch. The reason for the structural redundancy of the RC constitutes a central open question.[39]

The structure of the photosynthetic bacterial RC constituted a seminal accomplishment. Nevertheless, we should challenge the notion of the structure-function relationship providing a complete description of photosynthesis. Structural information alone is not sufficient to understand the function of the RC, which rests on the ingredients of ultrafast dynamics. Dynamic information transcendents and complements structural data. We should strive towards the broad unification of structure-dynamics-function relations in ultrafast biophysical and chemical dynamics.

References

1. G. R. Fleming, *Chemical Applications of Ultrafast Spectroscopy* (Oxford University, New York, 1986).
2. A. H. Zewail, *Femtochemistry* (World Scientific, Singapore, 1994).
3. R. Bersohn and A. H. Zewail, *Ber. Bunsenges. Phys. Chem.* 92 (1988) 373.

4. R. B. Bernstein and A. H. Zewail, *J. Chem. Phys.* **90** (1989) 829.
5. J. Jortner and R. D. Levine, *Isr. J. Chem.* **30** (1990) 207.
6. J. Purnell, E. M. Snyder, S. Wei and A. W. Castelman, *Chem. Phys. Lett.* **229** (1994) 333.
7. S. E. Bradforth, R. Jimenez, F. Van Mourik, R. Van Grondelle and G. R. Fleming, *J. Phys. Chem.* **99** (1995) 16179.
8. M. H. Vos, F. Rappaport, J. C. Lambry, J. Breton and J. L. Martin, *Nature* **363** (1993) 320.
9. M. Chachisvilis, T. Pullerits, M. R. Jones, C. N. Hunger and V. Sundström, *Chem. Phys. Lett.* **224** (1994) 345.
10. G. B. Kistiakowski and C. S. Parmenter, *J. Chem. Phys.* **42** (1965) 2942.
11. M. Bixon and J. Jortner, *J. Chem. Phys.* **48** (1968) 715.
12. M. Bixon and J. Jortner, *Mol. Cryst.* **213** (1969) 237.
13. M. Bixon and J. Jortner, *Isr. J. Chem.* **1** (1969) 189.
14. M. Bixon and J. Jortner, *J. Chem. Phys.* **50** (1969) 3284.
15. M. Bixon and J. Jortner, *J. Chem. Phys.* **50** (1969) 4061.
16. M. Bixon, Y. Dothan and J. Jortner, *Mol. Phys.* **17** (1969) 109.
17. S. Mukamel and J. Jortner, in *The World of Quantum Chemistry*, eds. R. Daudel and B. Pullman, Proc. First Intl. Congress Quantum Chemistry, pp. 145-209, Menton, France, 1973 (D. Reidel Publ. Co. 1974).
18. S. Mukamel and J. Jortner, in *MTP International Review of Science*, eds. A. D. Buckingham and C. A. Coulson (Butterworth, London, 1976) vol. 13, p. 327.
19. J. Kommandeur and J. Jortner, *Chem. Phys.* **28** (1978) 273.
20. J. Jortner and R. D. Levine, in *Advances in Chemical Physics* (Wiley, New York, 1981), vol. 47, pp 1-114.
21. A. Amirav, H. Horowitz and J. Jortner, *J. Chem. Phys.* **88** (1988) 3092.
22. J. Jortner, M. Bixon, H. Heitele and M. E. Michel-Beyerle, *Chem. Phys. Lett.* **179** (1992) 131.
23. M. Bixon and J. Jortner, *J. Phys. Chem.* **97** (1993) 13061.
24. J. Jortner and M. Bixon, *J. Photochem. Photobiol. A* **82** (1994) 5.
25. J. Jortner and M. Bixon, *J. Chem. Phys.* **102** (1994) 5636.
26. F. H. Mies and M. Kraus, *J. Chem. Phys.* **45** (1966) 4455.
27. I. McLaughlin, S. A. Rice and J. Jortner, *J. Chem. Phys.* **49** (1968) 2756.
28. J. Jortner, *Zeit. Phys. D* **24** (1992) 247.
29. J. Jortner, *Zeit. Phys. Chem.* **184** (1994) 283.
30. U. Buck and R. Krohne, *Phys. Rev. Lett.* **73** (1994) 947.
31. I. Schek, T. Raz, R. D. Levine and J. Jortner, *J. Chem. Phys.* **101** (1995) 8596.
32. A. Goldberg and J. Jortner (to be published).
33. J. Jortner, N. R. Kestner, M. H. Cohen and S. A. Rice, *J. Chem. Phys.* **43** (1965) 2614.
34. M. Rosenblit and J. Jortner, *Phys. Rev. Lett* **75** (1995) 4079.
35. R. Kubo, *Phys. Rev.* **86** (1952) 929.
36. R. A. Marcus, *J. Chem. Phys.* **966** (1956) 979.
37. K. J. Kaufman, P. L. Dutton, T. L. Netzel, J. S. Leigh and P. M. Rentzepis, *Science* **188** (1975) 1301.
38. J. Deisenhofer, O. Epp, K. Miki, R. Huber and H. Michel, *Nature* **318** (1985) 618.
39. M. E. Michel-Beyerle, M. Plato, J. Deisenhofer, H. Michel, M. Bixon and J. Jortner, *Biochim. Biophys. Acta* **932** (1988) 52.
40. R. A. Marcus, *Isr. J. Chem.* **28** (1988) 205.
41. M. Bixon, J. Jortner and M. E. Michel-Beyerle, *Biochem. Biophys. Acta* **1056** (1991) 301.
42. M. Bixon, J. Jortner and M. E. Michel-Beyerle, *Chem. Phys.* **197** (1955) 389.